PROPELLER SLIPSTREAM INVESTIGATION USING THE FOKKER F27 WIND TUNNEL MODEL WITH FLAPS DEFLECTED

M.J.T. Schroijen , L.L.M. Veldhuis , R. Slingerland
Department of Aerospace Design, Integration & Operations
Faculty of Aerospace Engineering
Delft University of Technology
P.O. Box 5058 2600 GB
Delft, The Netherlands
Phone: +31 152785293
M.J.T.Schroijen@tudelft.nl,
L.L.M.Veldhuis@tudelft.nl

Keywords: *Propeller, installation, vertical tail side wash*

Abstract

With the renewed interest in propeller propulsion because of environmental concerns, the need grows for a better understanding of the interaction effects of the propeller with the rest of the aircraft. The interaction of the propeller and wing with the vertical tail fin is of particular interest for directional control, especially with flaps deflected [14]. In order to obtain a better understanding of this interaction, wind tunnel tests have been performed in the wind tunnel at the Delft University of Technology (DUT). Three types of measurements have been performed on the 1:20 scale model of a Fokker F27, with flaps deflected. Forces and moments, side wash in front of the vertical tail, and the flow field behind the wing have been measured. These measurement results are used for comparison with and validation of a numerical aerodynamic model based on potential flow equations.

The measurements showed an increase in yawing moment of approximately 1.5 times the static yawing moment (thrust times moment arm) due to propeller installation effects. This increase was mainly caused by a side wash at the vertical tail due to the asymmetric lift distribution.
The displacement of the flap inner tip vortex was smaller than expected from previous numerical simulations, however the side wash induced by the wing trailing vortex sheet was larger.
A comparison of measurements, a RANS model and a potential method, showed that the difference in side wash between the methods is probably caused by a difference in calculated wing lift distribution, due to the negligence of wing thickness and propeller slipstream swirl reduction effects in the potential method.

Nomenclature

b	Wing span $[m]$
C_D	Drag coefficient $[-]$
C_n	Yawing moment coefficient $[-]$
C_T	Thrust coefficient $\frac{2T}{S_{ref}\rho V_\infty^2}$
D	Diameter $[m]$
E	Ratio between flap and total wing chord $\frac{c_f}{c_f+c_w}$
f	Propeller rotation frequency $[Hz]$
P	Pressure $[N/m^2]$
S	Surface area $[m^2]$
T	Thrust $[N]$
T_c	Thrust coefficient $\frac{2T}{S_p\rho V_\infty^2}$

v_t	Tangential flow velocity $[m/s]$
y_P	Propeller location in y-direction $[m]$
α	Angle of attack $[^\circ]$
β	Side slip angle, Blade angle $[^\circ]$

Subscripts

0	Without propeller
D	Dorsal fin
F	Fuselage
f	Flap
i	Installed
P	Propeller
S	Static
T	Tail
t	Total
u	Uninstalled
W	Wing
β	Derivative with respect to side slip angle

Abbreviations

CFD	Computational fluid dynamics
DUT	Delft University of Technology
IU	Inboard up
OEI	One engine inoperative
OU	Outboard up
RANS	Reynolds averaged Navier-Stokes
WTVS	Wing Trailing Vortex Sheet

1 Introduction

The rise in oil price and therefore in direct operating costs, increases the interest in more efficient ways of flying. Also, worldwide environmental concern is growing, particularly about the aviation sector's contribution to pollution. One solution to be investigated is the use of advanced high speed propellers. However, one of the major problems with propeller propulsion is the decreased aircraft stability and control in general and in one-engine-inoperative (OEI) conditions in particular. As early as the fifties Mannée noted that the yawing moment in OEI conditions can increase by as much as 100 percent with respect to the static yawing moment [14]. His explanation of increased side wash at the tail fin, due to the modified wing lift distribution, seems insufficient for conditions with flaps deflected, for it does not explain the large contribution by the fuselage as indicated by his own measurements. This condition of high thrust setting with large flap deflection condition, e.g. the go-around in approach setting, is the critical design condition for the fin. This is caused by the fact that the control forces on the fin are proportional to the flight speed squared and the thrust is approximately inversely proportional to the flight speed, resulting in large thrust effects with minimum ability for control at low speeds [13]. The complexity of the flow field behind the wing flap combination under the influence of the propeller has been investigated in reference [2] with qualitative measurements.

In order to gain a better understanding of the phenomena involved in the flow field behind the wing of a wing-fuselage combination with flaps deployed and one engine inoperative, wind tunnel measurements have been performed. Particular interest has been given to the cross flow in front of the vertical tail, and the region behind the wing with flaps deployed near the fuselage, in order to be able to compare the measured data to the results of the numerical model.

In the first section the measurements and results are explained. In the second section the potential model results are compared to the measurement data. In the third section the discrepancies in the numerical model and wind tunnel measurement data are evaluated further by employing a RANS (Fluent®) model. In the final section conclusions are drawn.

2 Measurements

Three types of measurements have been performed in the low speed, low turbulence wind tunnel at the DUT. Firstly forces and moments are measured to determine the power-on effects on the complete configuration. Secondly, side

wash was measured in front of the vertical tail to determine whether this could provide a sufficient explanation for the additional side force and yawing moment. Finally, the velocity vectors were determined behind the inboard wing, to capture the path of the inboard flap tip vortex and part of the propeller slipstream for a better understanding of the flow field behind the wing, inboard of the nacelle. These velocity vectors were obtained using a five-hole probe.

2.1 Model description

Model The wind tunnel model was a $1:20$ scale two engine Fokker F27 model ($b_W = 1.45m, l_F = 1.155m$), with double slotted in- and outboard flaps. The horizontal tail plane was removed for two reasons; to be able to measure in the flow field behind the wing and to reduce complexity by removing the interference effects as it has a stabilizing effect on the directional control [17, 18]. The two engines used to drive the two propellers ($D_P = 0.183m$) were high frequency three-phase induction motors rated at $3.6kW$.

Thrust setting To obtain a certain thrust setting, with the constant pitch propellers, comparable to go-around, the advance ratio $\left(\frac{V}{nD}\right)$ was kept as low as possible. This was obtained by choosing the highest practical propeller revolution speed ($280Hz$) and lowest free stream velocity ($40m/s$). The revolution speed was limited by engine cooling capacity and the free stream velocity by viscous effects. The resulting Reynolds number based on the wing chord of 350000 is quite low and transition strips at 30% of the wing and fin chord are used to prevent laminar separation of the boundary layer.

Other settings The measurements were performed with the flaps deflected as a whole over 24° at an angle of attack of 0° and 6° at a constant side slip angle of 0°.

2.2 Measuring equipment

Balance system The forces and moments are measured with the external six-component balance system. The model is connected to this balance system by three struts, two mounted at the wings and one at the aft body as can be seen in Appendix B, Figures 13 and 14. This aft body mount is also used to control the angle of attack of the model and to feed power and coolant to the engines. The model was inverted to minimize the disturbances by the mountings as can be seen in Figure 1.

Five-hole probe A five hole probe was used for the quantitative measurements in front of the vertical tail and behind the wing. The used five-hole probe had a diameter of $1.65mm$ and a conical head [23]. The probe was calibrated in the range of -45° to 45°. To reach all areas of interest if was positioned at 1.9° angle of attack and 11.9° angle of side slip. Moving the probe was done via an electronic traversing system.

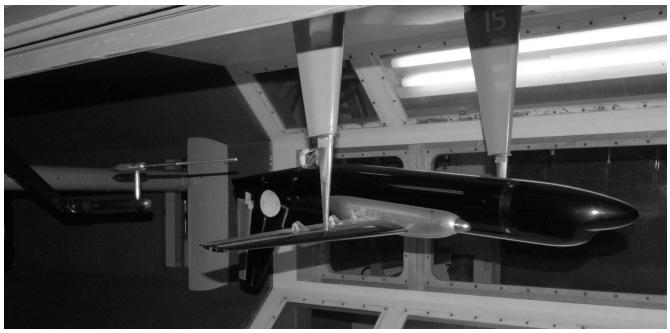

Fig. 1 The F27 model as mounted in the wind tunnel. In the back the five-hole probe and traversing system can be seen.

2.3 Measurement data processing

Balance measurements The balance measurements are corrected for wind tunnel wall and support interference effects. Zero measurements were performed to determine the forces and moments without propellers installed. These were subtracted from the forces and moments with one

propeller installed to determine the thrust coefficient

$$T_c = \frac{S_\infty}{S_P}\left(C_D(\alpha,\delta_f,J=0) - C_D(\alpha,\delta_f,J)\right). \quad (1)$$

The resulting thrust is actually the net (installed) thrust coefficient. The relation between advance ratio and net thrust coefficient is given in Figure 2.
The zero installed power measurements were also subtracted from the side force and yawing moment to correct for initial asymmetries in the model. Measurements were also performed for both the starboard and port engine to be able to correct for the thrust effect on the model asymmetries. The results for the side force and yawing moment from the starboard and port side are therefore averaged. The yawing moments are related to the static yawing moment. This static moment is defined as the net-thrust times the moment arm, and the yawing moment coefficient is defined by the difference in moment between the configuration without propeller and with running propeller. The resulting data are given in Figure 3 for the yawing moment and in Figure 4 for the side force coefficient.

Side wash measurements The velocity vectors are corrected for the slight asymmetries in the model and suspension, by performing a measurement without propellers installed and subtracting these values from the propeller operative values.

WTVS measurements The five hole probe was mounted such that one side of the wing trailing vortex sheet could be measured behind the propeller, wing and flap. To perform measurements on the opposite side of the operative engine, the propeller was uninstalled and installed on the opposite side instead of modifying the traversing system of the pitot probe. The measured velocities were calculated in the body frame of reference. To determine the vorticity strength a simple central difference scheme was used

$$\omega_{x(i,j)} = \frac{w_{i,j+1} - w_{i,j-1}}{\Delta y} - \frac{v_{i+1,j} - v_{i-1,j}}{\Delta z} \quad (2)$$

Table 1 Averaged additional yawing moment coefficient and side force coefficient, and resulting moment arm.

α		$\frac{\partial C_n}{\partial T_c}$	$\frac{\partial C_y}{\partial T_c}$	$\frac{l}{b}$
0°	IU	0.0122	−0.0422	0.289
	OU	0.0031	−0.0095	0.326
6°	IU	0.0211	−0.0488	0.432
	OU	0.0149	−0.0469	0.318

where v and w are the velocities in y and z direction respectively.

2.4 Results

The advance ratio thrust curve is given in Figure 2, the obtained thrust coefficients are small in comparison with Mannée. The thrusts for starboard, port, IU and OU rotating propellers are within a small band, showing that the thrust coefficient is independent of rotation direction and starboard or port placement on the wing. The results for the yawing moment obtained from the six component balance system are given in Figures 3 for an angle of attack of zero and six degrees. Combined with the side force coefficient, which is given in Figure 4, the moment arm of the additional yawing moment (ΔC_n) can be determined by,

$$\frac{l}{b} = -\frac{\Delta C_n}{\Delta C_y} = -\frac{\partial \Delta C_n}{\partial T_c}\frac{\partial T_c}{\partial \Delta C_y}, \quad (3)$$

Where Δ is the contribution due to the yawing moment excluding the static yawing moment. The averaged results are given in Table 1. The moment arm is close to the moment arm of the vertical tail plane ($\frac{l_T}{b} = 0.390$) from which it can be concluded that the additional side force and yawing moment coefficient are mainly caused by a contribution of the vertical tail plane.

The vertical tail plane contribution to the yawing moment and side force is probably

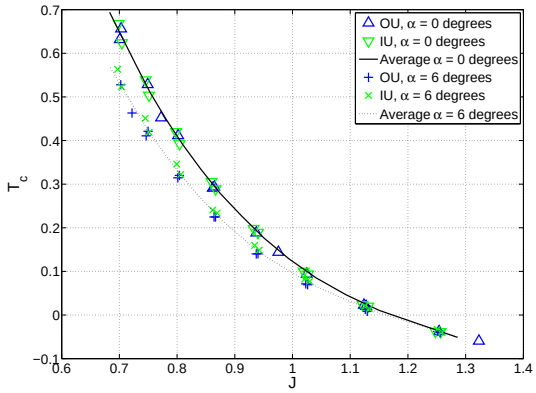

Fig. 2 Advance ratio versus thrust curve for the Fokker F27 configuration with flaps deflected at $\alpha = 0^\circ$ and 6°.

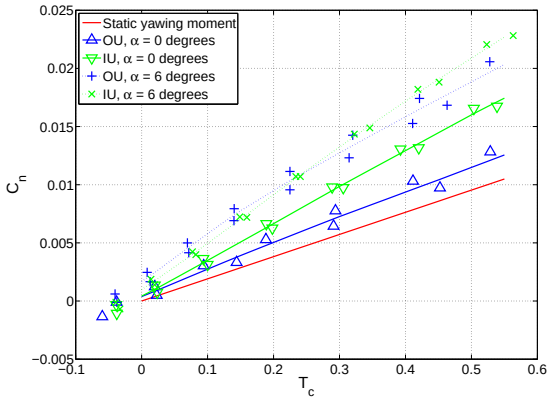

Fig. 3 Thrust versus yawing moment curve for the Fokker F27 configuration with flaps deflected at $\alpha = 0^\circ$ and 6°.

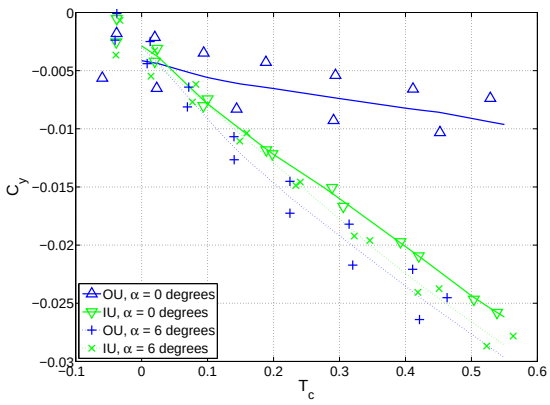

Fig. 4 Thrust versus side force curve for the Fokker F27 configuration with flaps deflected at $\alpha = 0^\circ$ and 6°.

Table 2 Equivalent side wash at the tail due to the propeller. For two angles of attack and one propeller speed, $f = 280Hz$

α		ΔC_n	$\left(\frac{\partial C_n}{\partial \beta}\right)_T$	$\bar{\beta}$	$\beta[^\circ]$
0°	IU	0.0053	0.219	0.024	1.4
	OU	0.0025	0.219	0.011	0.6
6°	IU	0.0083	0.226	0.037	2.1
	OU	0.0070	0.226	0.031	1.8

caused by an increased side wash. Approximating an equivalent side slip angle can be done by applying the following formula, for a motor frequency of $280Hz$,

$$\frac{\Delta C_n}{\beta} \approx \left(\frac{\partial C_n}{\partial \beta}\right)_T, \tag{4}$$

again the Δ represents the additional yawing moment coefficient without the static yawing moment. The stability derivative for the tail is measured in reference [4] and the results for the equivalent side slip angle are given in Table 2. The procedure employed is explained in more detail in Section 2.5. Comparing the results to the measured values of side wash at the vertical tail, given in Figure 5. The equivalent values are leaning towards the higher side of the side wash. This might be caused by the fact that the side wash is largest near the root of the fin which is also the location of the largest lift production (e.g. large chord, fuselage effect) as can be seen in Figure 6. The approximated vertical tail lift distribution as calculated by a Prantl's lifting line theory and the measured side wash including the contribution of the fuselage on the vertical tail is given in Figure 6. These results support the conclusion that the additional yawing moment is caused by the vertical tail.

The additional yawing moment and side force are caused by the vertical tail plane subjected to side wash, however the cause for this side wash is still to be determined. According to Mannée this

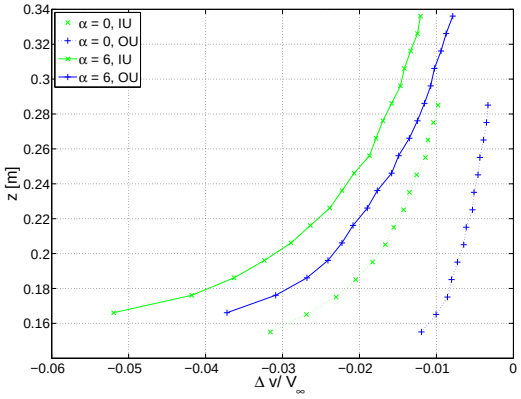

Fig. 5 Non-dimensional side wash in front of the vertical tail for two angles of attack and rotation directions, $f = 280Hz$.

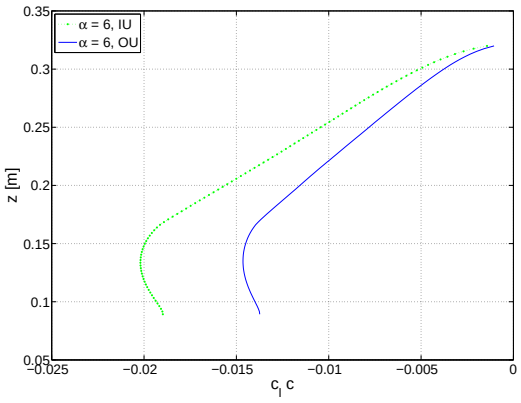

Fig. 6 Lift distribution on the fin at $\alpha = 6^\circ$ calculated with the measured side wash.

side wash is caused by the asymmetrical wing lift distribution. Two contributions are assumed, first the side wash due to an asymmetrical vortex strength distribution of the wing trailing vortex sheet and second the asymmetrical shape of the vortex field due to the asymmetrical roll up of the sheet. Both effects are closely related and cannot be seen completely separate.

The first effect is closely related to the lift distribution on the wing, this relation can also be seen when comparing the side wash measurements for zero and six degrees angle of attack. Increasing the angle of attack increases the lift and therefore the strength and asymmetry of the wing lift distribution, resulting in a larger side wash at the vertical tail at larger angles of attack (Figure 5).

The second effect is closely related to the asymmetric movement of the flap tip inner vortex due to the wing trailing vortex sheet and fuselage effect. From references [19] and [20] it was found that the position of the flap inner vortex has a major contribution to the side wash at the vertical tail plane and was therefore tracked along the fuselage at four stations as indicated in Appendix B, Figure 13. The flap inner vortex positions are given in Figure 7 for zero and six degrees angle of attack. Only the figures for IU rotation are given as this is the most critical configuration. The positions of the flap inner vortex differ for the working propeller side and the propeller inoperative side, however the displacements are smaller than expected from references [19] and [20], which might be caused by the smaller thrust settings obtained in the measurements. However a more likely explanation is the overestimation of the fuselage contribution to the vortex displacement in the numerical potential model due to the singularities inherent to the the wing trailing vortex sheet model based on discrete vortex elements.

2.5 Notes

The thrust coefficients obtained with the current test setup were far below the thrust coefficients employed during take-off or go-around. However

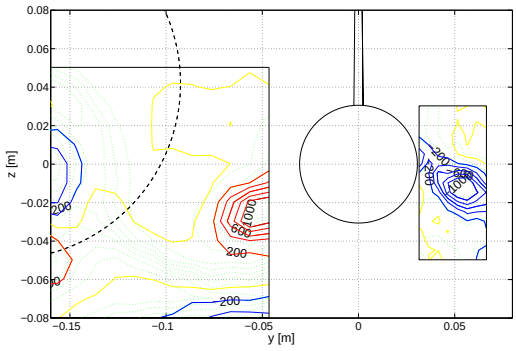

(a) $\alpha = 0^\circ$

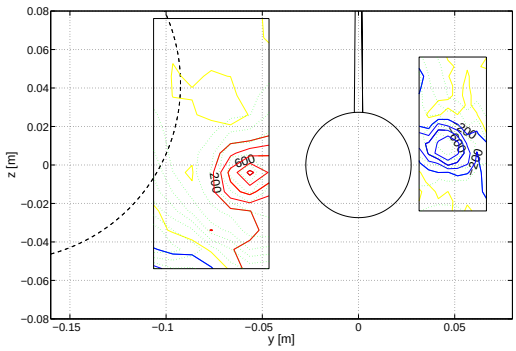

(b) $\alpha = 6^\circ$

Fig. 7 Flap inner vortex position at the vertical tail plane (Station 4), at $f = 280Hz, IU, \alpha = 6^\circ$ as seen from the back, left side is the operating engine side (IU).

a factor k of about 2 ($\alpha = 6^\circ, IU, T_c = 0.4$) has to be used for the increase in yawing moment

$$k = \frac{C_n}{C_{n_S}}. \tag{5}$$

Tail and dorsal fin contribution The contribution of the vertical tail plane and dorsal fin to the yawing moment has been estimated by comparing the side wash measured in front of the vertical tail to the effect of an angle of side slip change. The measured yawing moment coefficient derivatives (C_{n_β}) for the complete configuration can be subtracted from the measured values for the configuration without tail or dorsal fin to find the contribution of the vertical tail to the yawing moment,

$$\left(C_{n_\beta}\right)_{TD} = \left(C_{n_\beta}\right)_{WFTD} - \left(C_{n_\beta}\right)_{WF} \tag{6}$$

Table 3 Measured yawing moment coefficient derivatives with respect to sideslip angle for various components of the aircraft [4].

α	$\left(C_{n_\beta}\right)_{WFTD}$	$\left(C_{n_\beta}\right)_{WF}$	$\left(C_{n_\beta}\right)_{TD}$
-0.8°	0.146	−0.073	0.219
5.5°	0.163	−0.063	0.226

The results for an angle of attack of -0.8° and 5.5° can be found in Table 3. The effect of the dorsal fin on the vertical tail yawing moment contribution is negligible [4]. The fuselage support was found to have a yawing moment increasing and side force decreasing effect due to side slip acting as an increase of vertical tail surface area. According to Mannée [13] however the effect would be decreasing for the propeller moment, the measured results are therefore assumed to be a slight underestimation.

3 Potential flow model

The measurement data presented in the previous section are used to validate the numerical aerodynamic model based on potential methods [19, 20]. The propeller is modeled by vortex theory [9] with a correction for the finite number of blades [5], the wing and flap by Prandtl's lifting line theory including the interaction with the fuselage [8, 11, 16] and the deformation of the wing trailing vortex sheet is computed by a fourth order Runge-Kutta time stepping method [3, 12].

3.1 Results

The yawing moment coefficients as calculated by the potential flow model are given in Figure 8 for $\alpha = 0^\circ$ and $\alpha = 6^\circ$. For both angles of attack there is a significant difference in measured and

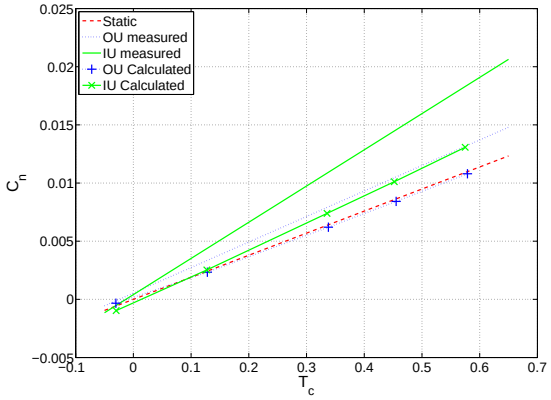

(a) $\alpha = 0^\circ$

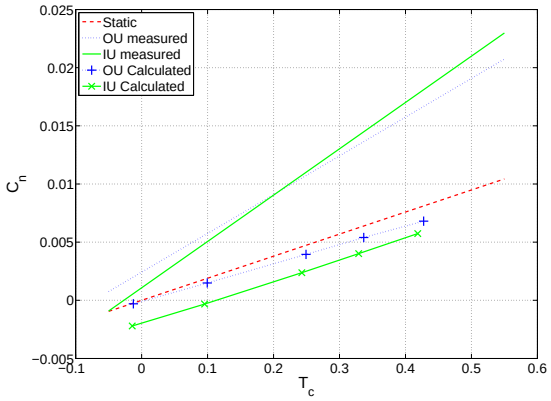

(b) $\alpha = 6^\circ$

Fig. 8 Yawing moment coefficient as measured and calculated.

computed yawing moment coefficient. To investigate the difference in yawing moment the contributions of the various components are investigated. As mentioned in section 2.4 the contribution of the vertical tail can be modelled with an equivalent side slip angle and a yawing moment and side force derivative.

$$C_n = C_{n_\beta}\bar{\beta} \tag{7}$$

The aircraft was put at a finite sideslip angle to determine the side force and yawing moment derivative. The side force and yawing moment derivatives with respect to this side slip angle are subsequently compared to the data obtained from reference [4] to see whether for the same forces and moments are obtained. The second cause for the difference in yawing moment is a difference in side wash at the vertical tail which will be evaluated next.

Side slip angle derivatives

Wing and fuselage contribution To be able to determine the contribution of the vertical tail to the yawing moment coefficient, the contributions due to the fuselage and wing have to be estimated first. The results for the yawing moment coefficient derivative and side force derivatives are given in Table 4 (Upper part, index WF). The results from reference [4] as well as the results computed by the ESDU method [6] are shown. The yawing moment derivative of the potential model agrees well to the measured and computed ESDU values. The side force derivative however is largely underestimated which is probably caused by neglecting viscous effects (vortex formation and flow separation) on the front and aft part of the fuselage [15]. The nacelle influence and the fact that the fuselage is approximated by a cylinder instead of the actual more elliptic shape are also a cause for errors in fuselage contribution [10]. Furthermore the compensating effect of the wing on the yawing moment derivative was found to be lower than expected from reference [10]. Most sources for error are found to be determined by the contribution of the nose of the fuselage at an angle of yaw. The OEI

measurements however have been performed using zero side slip angle, where these sources of error do not occur and the model produces valid results for the contribution of the fuselage-wing combination.
According to reference [22] the contribution of the nacelles is negligible in OEI conditions and is therefore not treated separately however the effects are taken into account by the potential flow model.

Vertical tail contribution The contribution of the vertical tail to the side force and yawing moment derivative are obtained by subtracting the values for wing and fuselage from the total side force and yawing moment derivatives. These values therefore include the additional contribution due to the fuselage-fin interaction and are presented in Table 4 (Lower part, index T). The ESDU method employed is given in reference [7].

Conclusion The side slip derivatives compare quite well to the measured ones. Therefore the conclusion is drawn that the error in yawing moment prediction as indicated in Figures 8 in one engine inoperative conditions is probably not caused by the modelling of the components at an angle of side slip. The cause for difference is therefore sought in an error in calculated side wash.

Side wash

The side wash as calculated by the potential model is smaller than measured in the wind tunnel as can be seen from a comparison of Figures 5 and 9. Striking is the fact that the calculated side wash for zero angle of attack is larger than the six degrees angle of attack for inboard up rotation. The calculated side force due to the vertical tail is therefore smaller as well as the resulting increase in yawing moment. The side wash is mainly due to the strength and shape of the vortex field. The results of the potential model for IU rotation for both angles of attack are given in Figure 10. Comparing these results to the mea-

Table 4 Comparison of the directional stability derivatives, $\alpha = 0\,^\circ$.

	$\left(C_{n_\beta}\right)_{WF}$	$\left(C_{Y_\beta}\right)_{WF}$
Ref. [4]	-0.073	-0.1709
ESDU	-0.054	-0.1679
Model	-0.092	-0.0736
	$\left(C_{n_\beta}\right)_{T}$	$\left(C_{Y_\beta}\right)_{T}$
Ref. [4]	0.231	-0.696
ESDU	0.289	-0.794
Model	0.233	-0.629

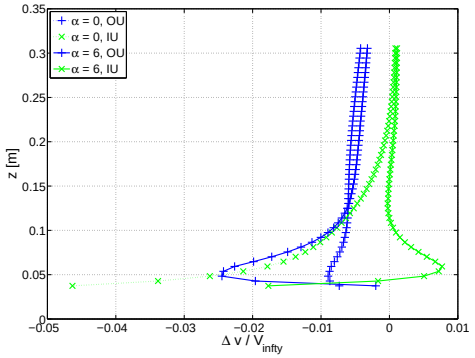

Fig. 9 Side wash at the vertical tail plane as calculated with the potential method.

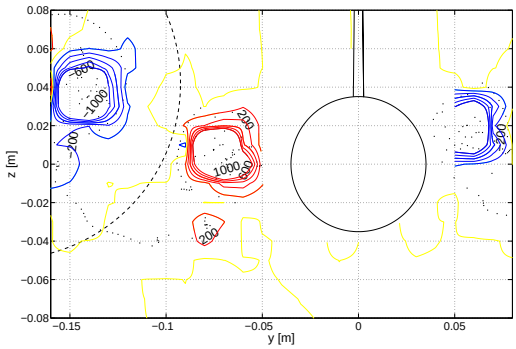

(a) $\alpha = 0^\circ$

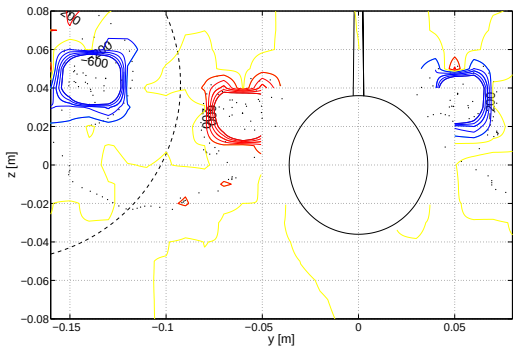

(b) $\alpha = 6^\circ$

Fig. 10 Flap inner vortex position at the vertical tail plane as calculated by the potential model, at $f = 280Hz, IU$ as seen from the back, left side is the operating engine side (IU).

surement data (Figure 7) a difference in vorticity strength and distribution can clearly be seen. This is probably caused by a discrepancy in lift distribution as well as an effect of dividing the continuous sheet into discrete elements. To investigate this discrepancy further a CFD model has been made, which is discussed in the next section.

3.2 Notes

One of the major problems with potential methods are the singularities imposed by the mathematical elements used to describe the flow field. Dividing into singular elements works as long as the positioning of the elements is fixed, can be controlled or disturbances are small. In the free wake model the approximation of the continuous vorticity sheet by discrete elements becomes a problem when elements are close to each other (collocation points). In order to smooth out the singularities viscous effects are included by applying a concrete viscous core [21]. The free wake models are therefore only applicable when the point of interest is relatively far away from the discrete vortex field, which is approximately 2 times the width of the original vortex distribution which is modelled as one vortex [11]. With the inner flap end vortex relatively far away from the vertical tail plane this approximation is still valid, for the velocities on the fuselage this is not trivial.

4 CFD model

In order to investigate the discrepancy between the measurements and numerical model further a simple computational model has been made using the Fluent® flow solver to model the configuration as measured by Mannée. The simplification of the problem with the laminar flow was meant as a first acceptable estimate.

The propeller disc was modeled with the build in function of the fan, which allowed for a variable tangential velocity distribution aft of the propeller disc which was calculated as a actuator disc. To obtain the correct installed thrust as used by Mannée the uninstalled thrust is varied in the vortex theory propeller model. This produces; the pressure jump averaged over the propeller disc (ΔP) and the tangential velocity distribution represented as a function of radius ($v_t(r)$), which are used as input in the Fluent® fan model. With this model the drag coefficient is obtained which is again used as input for the propeller model until the correct installed thrust is obtained. The results of Figure 11 show an overestimation for both inboard and outboard rotation. The problem is probably caused by numerical diffusion due to the rather coarse grid, which was chosen to limit the computing time required. An Euler approximation suffers less from diffusion and might give a better approximation. However the trend is similar to the measured one, making it still useful for

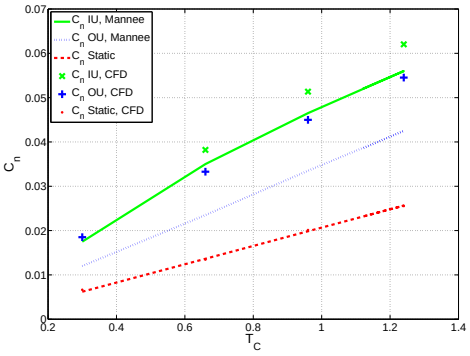

Fig. 11 The yawing moment coefficient, measurements by Mannée and computations based on the combined RANS model (CFD).

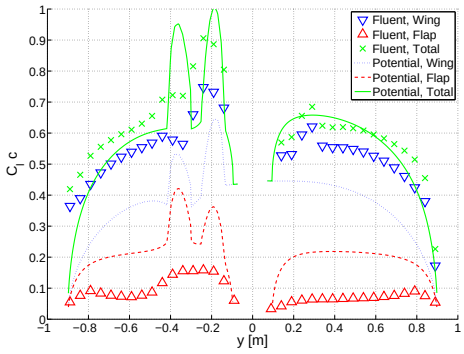

Fig. 12 Wing and flap lift distribution as calculated by the Fluent model and potential method for the configuration as used by Mannée.

design purposes.

The good correspondence of the yawing moment coefficients as measured and calculated by the Fluent® solver shows that the CFD model can be used for comparison and that separation and turbulence of the boundary layer are not of primary interest. As mentioned in the previous section the wing lift distribution might be modelled incorrectly resulting in a dissimilar cross flow at the tail. Comparing the lift distribution as computed with the RANS model and the potential model has been done in Figure 12. Comparing the inflow velocities in front of the wing and correcting the Fluent® inflow for the upwash caused by the wing the following can be concluded: the inflow velocities are similar, however negligence of the nacelles, thickness effects and propeller slipstream swirl reduction on the flap are main causes for the differences in lift distribution.

A second observation is the fact that the wing lift distribution seems underestimated by the potential method and the flap lift distribution overestimated. The fact that the flap carries most of the additional load is due to the simple 2 lifting line model (one over the wing and one over the flap which are coupled). The additional overall load due to the flap deflection [19]

$$\frac{\partial \alpha}{\partial \delta} = \frac{3E}{2E+1}, \tag{8}$$

is however comparable to the measurement results of reference [1]. E is defined as the ratio between the flap chord and total (wing + flap) chord. The total wing lift with the contribution of the flap is therefore expected to be similar, and has been verified by adding more horseshoe vortices in chordwise direction. The chordwise distribution of load varied significantly whereas the total load remained fairly similar.

5 Conclusions

As was expected from the measurements performed by Mannée, the yawing moment coefficient with flaps deflected and one engine inoperative is significantly, approximately 1.5 times, larger than the static yawing moment (thrust times moment arm). The wind tunnel measurements presented in this paper were performed with a thrust coefficient which is relatively small for take-off conditions, however the trend of the yawing moment increment due to the propeller slipstream interaction is clear. The most probable cause for this increment in yawing moment is the increased side force on the fin due to the asymmetrical lift distribution over the wing/ flap due to the propeller slipstream. This wing lift distribution gives rise to an asymmetrical wing trailing vortex sheet roll-up which adds to the asymmetry of the flow field. The asymmetric wing trailing vortex sheet induces a side wash at the fin location resulting in an

additional contribution of the fin to the yawing moment.

The effects of the flap inner vortices on the fuselage were smaller than expected from previous numerical simulations, as were the displacements of the flap inner vortex due to the thrust setting. However the contribution of the asymmetry of the wing trailing vortex sheet to the side wash on the fin was underestimated. Therefore a more detailed study has to be performed on both the shape and strength of the wing trailing vortex sheet.

Comparing the potential model results to the measurements it is found that the calculated yawing moment is generally underestimated. This is caused by a difference in lift distribution over the wing flap combination. This difference is probably caused by neglecting wing thickness effects and propeller swirl reduction. The difference in lift distribution causes a difference in both strength and shape of the wing trailing vortex field. Adding to this are the discontinuities inherent in potential flow modelling (vortex model). All these factors result in an underestimation of the side wash at the fin and therefore an underestimation of the fin's contribution to the yawing moment.

The results for the RANS simulation are encouraging with respect to the critical inboard up rotation case; the differences with measurement results are very likely to be caused by numerical dissipation due to a rather coarse grid chosen to keep calculation time to a minimum. Additional CFD calulations using low dissipative schemes should be used to improve the computed results.

5.1 Copyright Statement

References

[1] I.H. Abbot and A.E. von Doenhoff. *Theory of wing sections*. Dover publications inc., second edition, 1959.

[2] A.S. Aljabri and A.C. Hughes. Windtunnel investigation of the interaction of propeller slipstream wih nacelle/wing/flap combinations. Paper AGARD FDP 366-21, AGARD, 1984.

[3] A. Betz. Behavior of vortex systems. Technical Memorandum 713, National Advisory Committee for Aeronautics, 1932.

[4] H. Brinkhorst. Windtunnelmetingen aan een model van de Fokker F-27 "Friendship" in de lage-snelheidstunnel van de onderafdeling vliegtuigbouwkunde. Memorandum M 47, Technische hogeschool Delft, 1961.

[5] W.F. Durand, editor. *Aerodynamic theory*, volume IV. Springer, 1935.

[6] Engineering Sciences Data Unit. *ESDU 79006: Wing body yawing moment and sideforce derivatives due to sideslip: N_v and Y_v (With addendum for nacelle effect)*.

[7] Engineering Sciences Data Unit. *ESDU 82010: Contribution of fin to sideforce, yawing moment and rolling moment derivatives due to sideslip, $(Y_v)_F$,$(N_v)_F$,$(L_v)_F$, in the presence of body, wing and tailplane*.

[8] J.P. Giesing. Lifting surface theory for wing-fuselage combinations. Report DAC 67212, Douglas Aircraft company, 1968.

[9] H. Glauert. *The elements of aerofoil and airscrew theory*. Cambridge University Press, second edition, 1947.

[10] R.O. House and A.R. Wallace. Wind-tunnel investigation of effect of interference on lateral-stability characteristics of four naca 23012 wings, an elliptical and a circular fuselage and vertical fins. Report 705, National Advisory Committee for Aeronautics.

[11] J. Katz and A. Plotkin. *Low speed aerodynamics*. Cambridge university press, second edition, 2001.

[12] R. Krasny. Computation of vortex sheet roll-up

in the trefftz plane. *Journal of Fluid mechanics*, (184):123–155, 1987.

[13] J. Mannée. Windtunnel investigation of the influence of the aircraft configuration on the yawing- and rolling moments of a twin-engined propeller driven aircraft with one engine inoperative. Report NLL A-1508 B, NLL, 1962.

[14] J. Mannée. Windtunnel onderzoek naar de invloed van de vliegtuigconfiguratie op gier- en rolmoment ten gevolge van het uitvallen van een motor bij een tweemotorig schroefvliegtuig. Report NLL A-1508 A, NLL, 1963.

[15] H.K. Millicer. Sidewash and stability, a study of wing/fuselage interference effects. *Flight*, 27 July 1950.

[16] H. Multhopp. Aerodynamics of the fuselage. Technical Memorandum 1036, National Advisory Committee for Aeronautics, 1942.

[17] A. van Nispen. Slipstream effects on the static lateral and directional control of a multi-engined propeller aircraft with one engine inoperative. Master's thesis, Delft university of technology, 2002.

[18] A. van Nispen and R. Slingerland. Propeller slipstream effects on lateral and directional controllability of multi-engined aircraft. Paper, Society of flight test engineers, 2002.

[19] M.J.T. Schroijen and R.Slingerland. Propeller slipstream effects on directional aircraft control with one engine inoperative. Report AIAA 2007-1046, American Institute of Aeronautics and Astronautics, 2007.

[20] M.J.T. Schroijen and R. Slingerland. Propeller installation effects on multi-engine propeller aircraft directional stability and control. Paper 6.10.2, International Council of the Aeronautical Sciences, 2006.

[21] A. von Timme. Uber die Geschwindigkeitsverteiling in Wirbeln. Report Band XXV, Archive of Applied Mechanics, Ingenieur Archiv, 1957.

[22] R. S. van Rooyen and M. E. Eshelby. Assessment of propeller influence on lateral-directional. stability of multiengine aircraft. *Journal of Aircraft*, 18(4):364–371, 1981.

[23] L.L.M. Veldhuis. *Propeller wing aerodynamic interference*. Phd thesis, Delft University of Technology, 2005.

A Necrologie

On Friday the 19th of November the co-author of this paper, Ronald Slingerland (46), died in an accident during which his plane collided with another small aircraft. The plane lost a section of its tail and was damaged beyond recovery. He was flying the plane together with his colleague Poppe de Lange (70), who also lost his live in this tragic accident. They both will be missed.

Ronald gave lectures on preliminary designs for aircraft and ran design exercises, alongside a whole host of other teaching and research activities. His extraordinary lectures were peppered with his practical knowledge of flying. He would combine his wealth of experience from working as a member of the team of preliminary designers at Fokker with an almost encyclopedic knowledge of aircraft.

For us Ronald has been an exceptional tutor an colleague. He gave the first author the inspiration to start a PhD and many discussions were held on the subject. Furthermore he always managed to keep his students and colleagues motivated with his ever lasting enthusiasm no matter how disappointing the results.

B Wind tunnel model dimensions

The model used for the wind tunnel measurements is an 1:20th scale Fokker F27, with double slotted flaps and a removable horizontal tail. For the measurements this horizontal tail has been removed for several reasons, one of them being able to measure in front of the vertical tail plane. All dimensions are in *mm*.

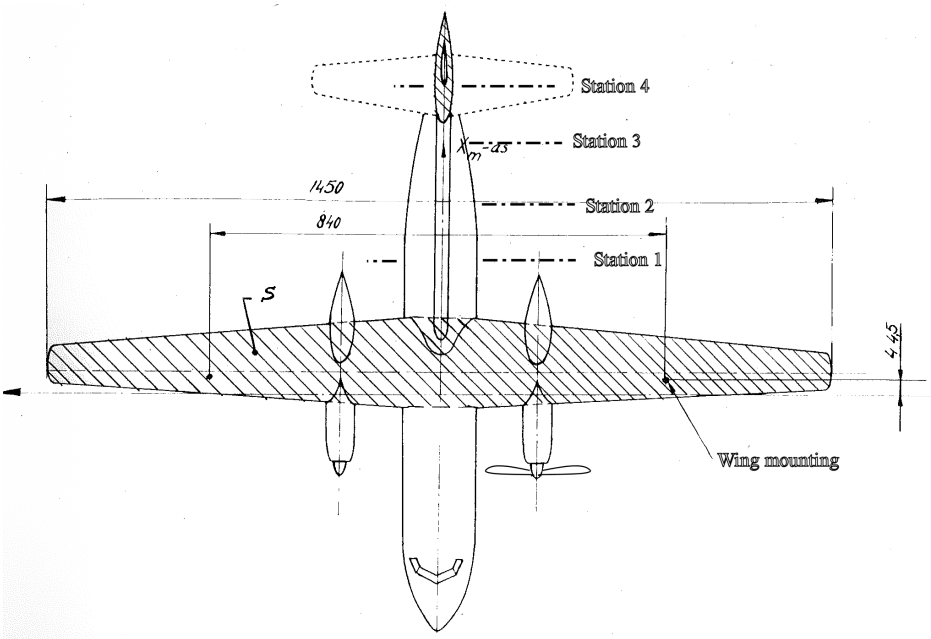

Fig. 13 F27 model with mounting points, and the stations used for flow measurements behind the wing, adapted from reference [4].

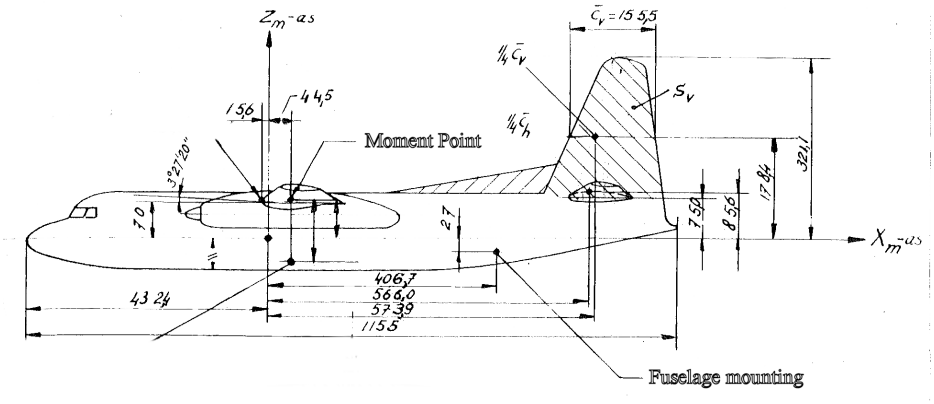

Fig. 14 F27 model and mounting points, the moment point is also the wing mounting point adapted from reference [4].